

An Adaptive Multigrid Solver for Applications in Computer Graphics

Misha Kazhdan¹ and Hugues Hoppe²

¹Johns Hopkins University ²Google Inc.

Supplementary Results

This supplemental material shows additional results of our adaptive solver for applications in surface reconstruction, gradient-domain image stitching, and Euclidean distance transform computation.

Figure 9 compares the results of our degree-one (first column) and degree-two (second column) implementations of Screened Poisson Reconstructions, as well as implementations of Smoothed Signed Distance reconstruction by Calakli *et al.* (third column) and using our adaptive solver (final column).

Figure 10 shows the input image composite with a false color visualization of the individual images (left) and the result of our gradient-domain image stitching (right).

Figure 11 compares close-ups from the Jerusalem panorama stitching results (Figure 7 in the main text) using different under-relaxation parameters.

Figure 12 compares the exact distance transform obtained using the method of Saito and Toriwaki (left) with the distance transform obtained using our implementation of Geodesics-in-Heat (right).

Figure 13 compares close-ups from the Euclidean distance transform obtained from the bunny model (Figure 8 in the main text) using different under-relaxation parameters.

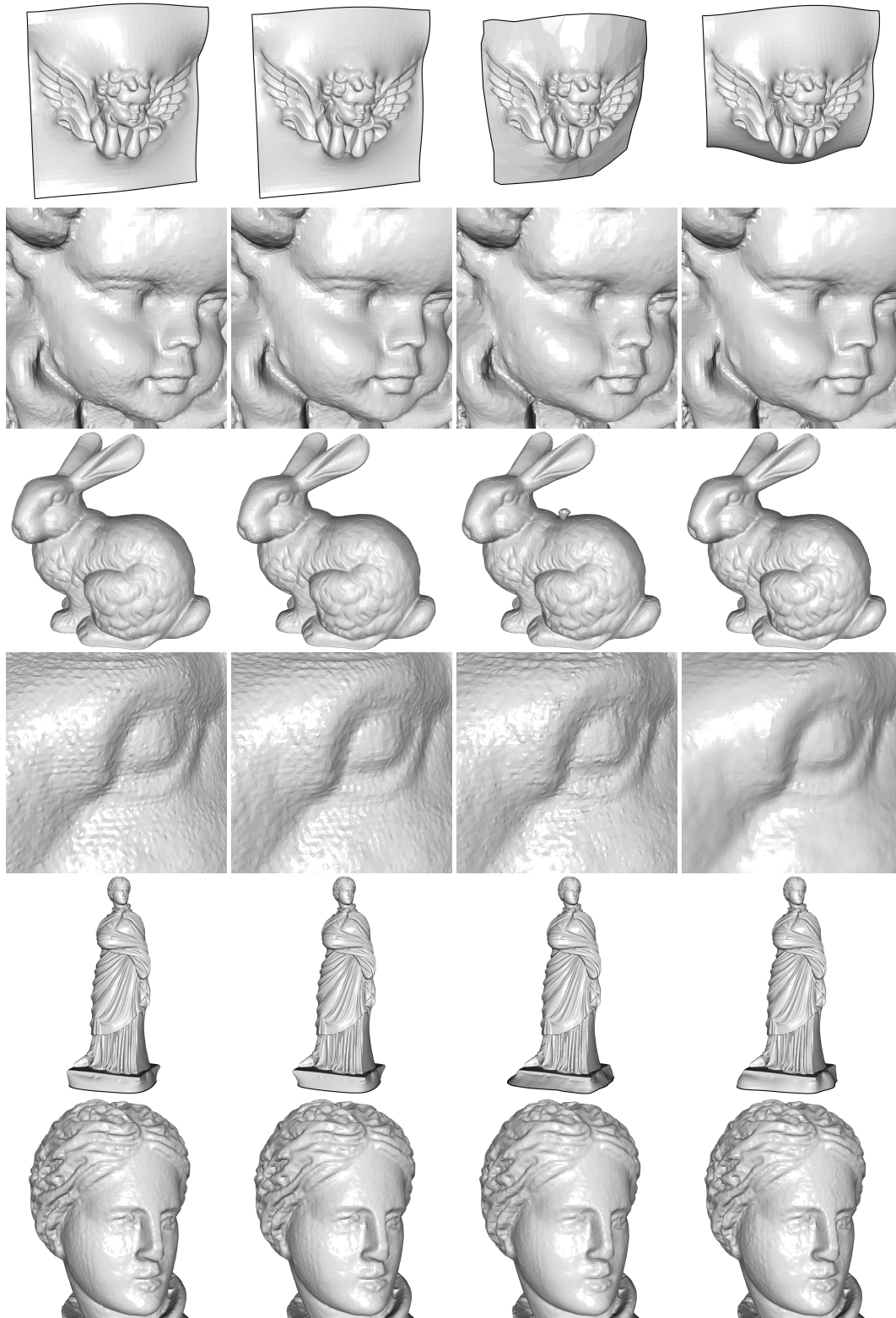


Figure 9: Surface reconstructions, showing (from left to right) the results of the Screened Poisson Reconstruction (degree 1), Screened Poisson Reconstruction (degree 2), the original implementation of the Smoothed Signed Distance Reconstruction by Calakli *et al.*, and our implementation of the Smoothed Signed Distance Reconstruction.

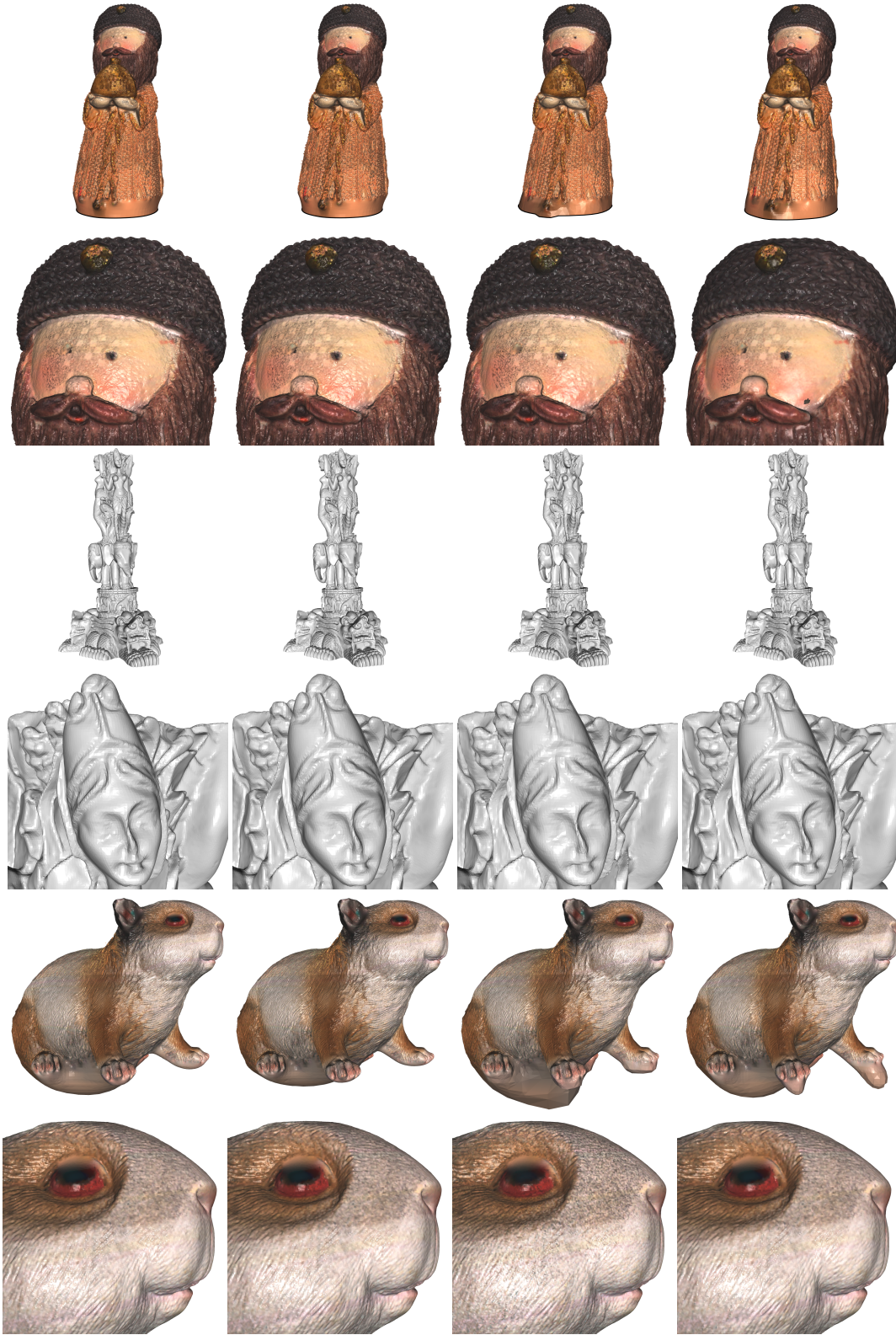


Figure 9: Surface reconstructions, showing (from left to right) the results of the Screened Poisson Reconstruction (degree 1), Screened Poisson Reconstruction (degree 2), the original implementation of the Smoothed Signed Distance Reconstruction by Calakli *et al.*, and our implementation of the Smoothed Signed Distance Reconstruction.

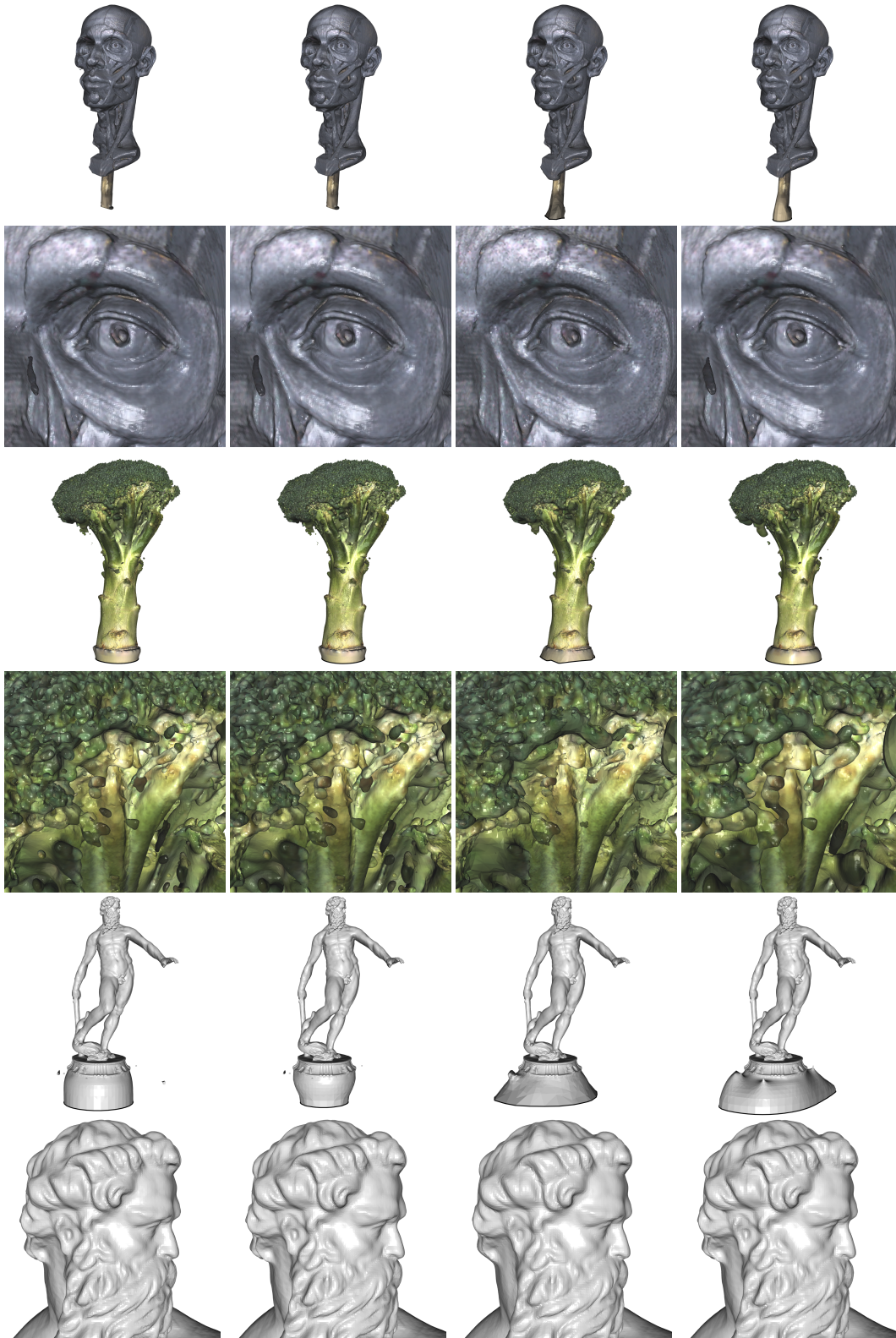


Figure 9: Surface reconstructions, showing (from left to right) the results of the Screened Poisson Reconstruction (degree 1), Screened Poisson Reconstruction (degree 2), the original implementation of the Smoothed Signed Distance Reconstruction by Calakli *et al.*, and our implementation of the Smoothed Signed Distance Reconstruction.

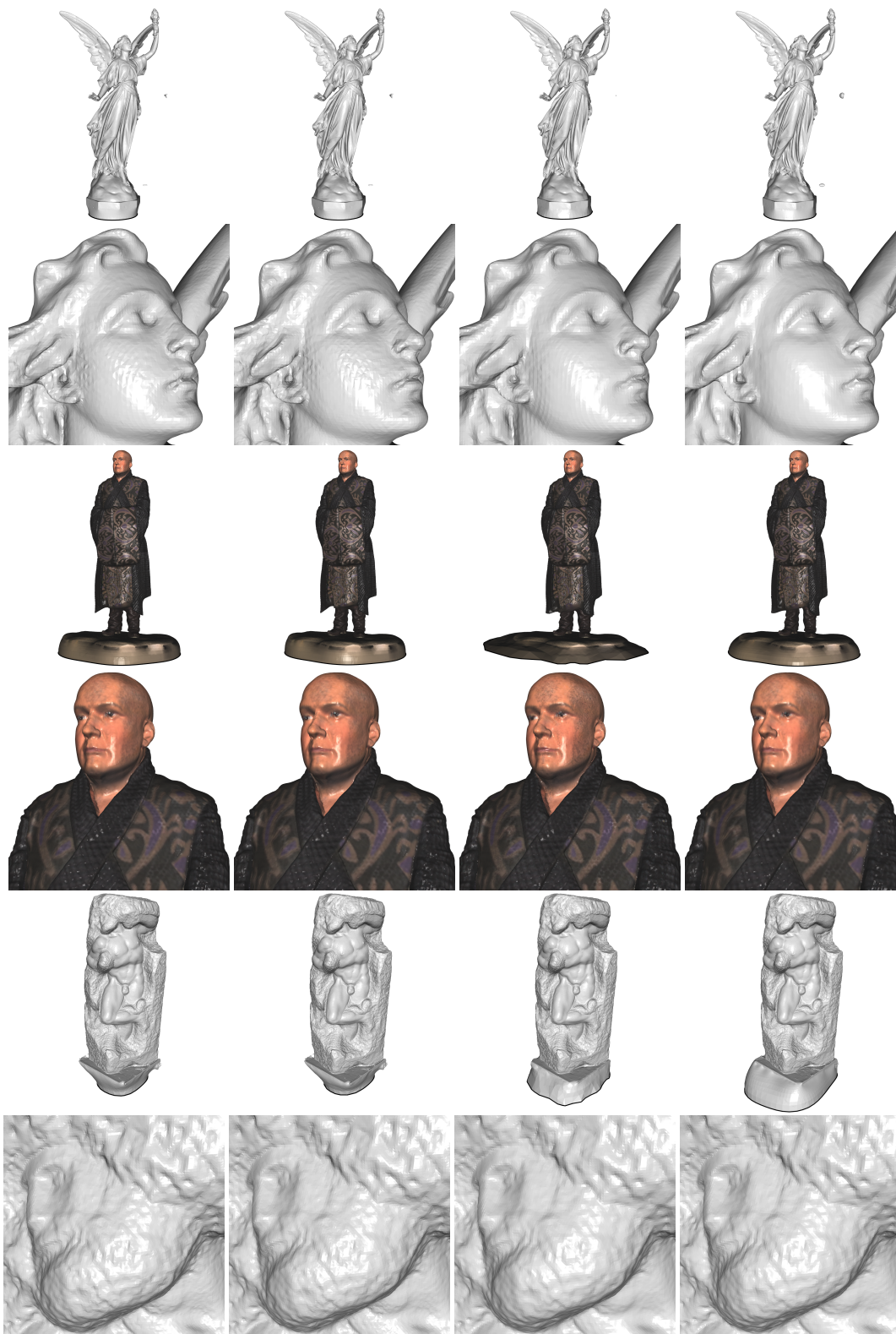


Figure 9: Surface reconstructions, showing (from left to right) the results of the Screened Poisson Reconstruction (degree 1), Screened Poisson Reconstruction (degree 2), the original implementation of the Smoothed Signed Distance Reconstruction by Calakli *et al.*, and our implementation of the Smoothed Signed Distance Reconstruction.

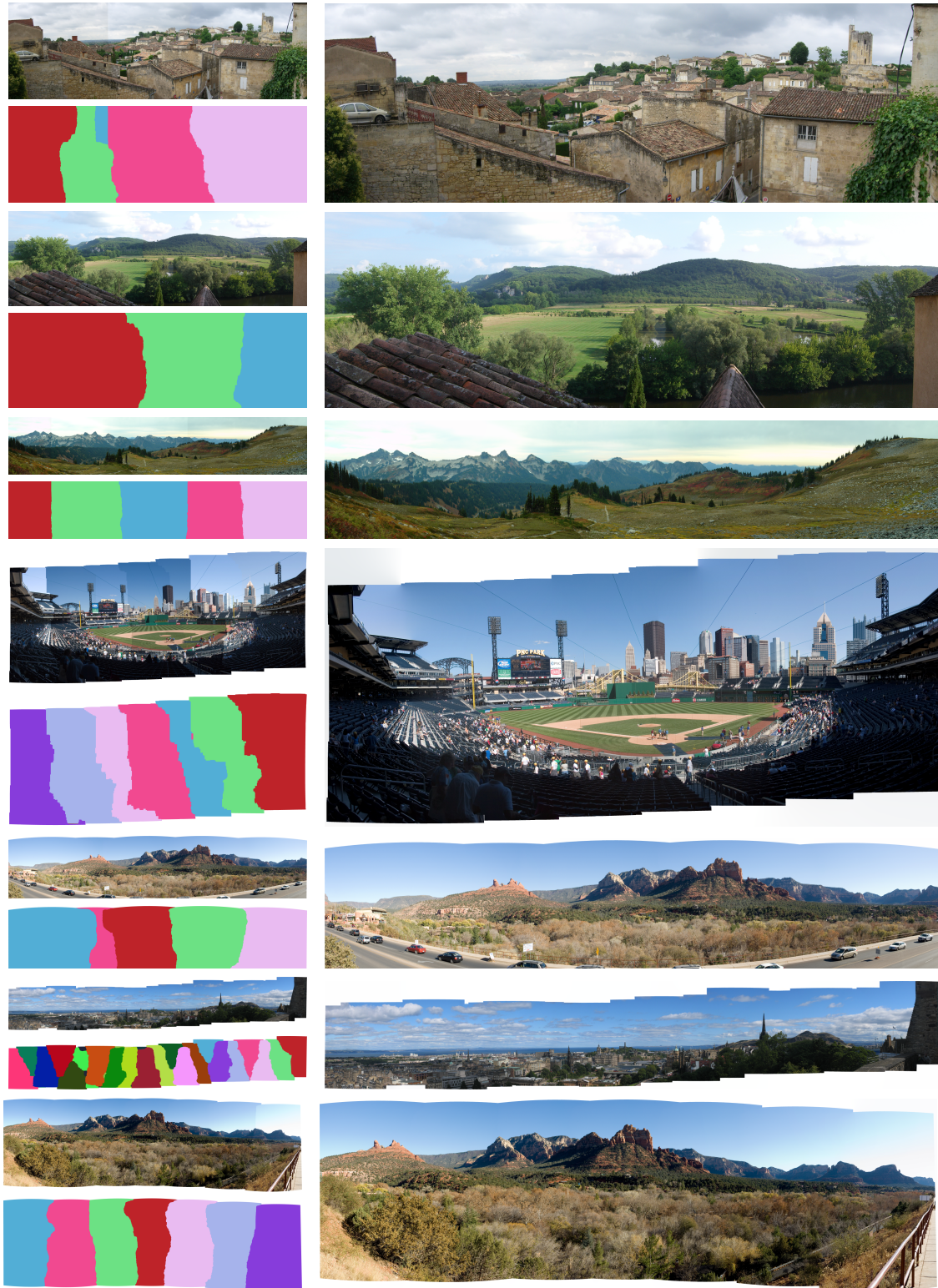


Figure 10: Image stitching results, showing the input composite and assignment mask making up the panorama (left), and the output (right).



Figure 10: Image stitching results, showing the input composite and assignment mask making up the panorama (left), and the output (right).

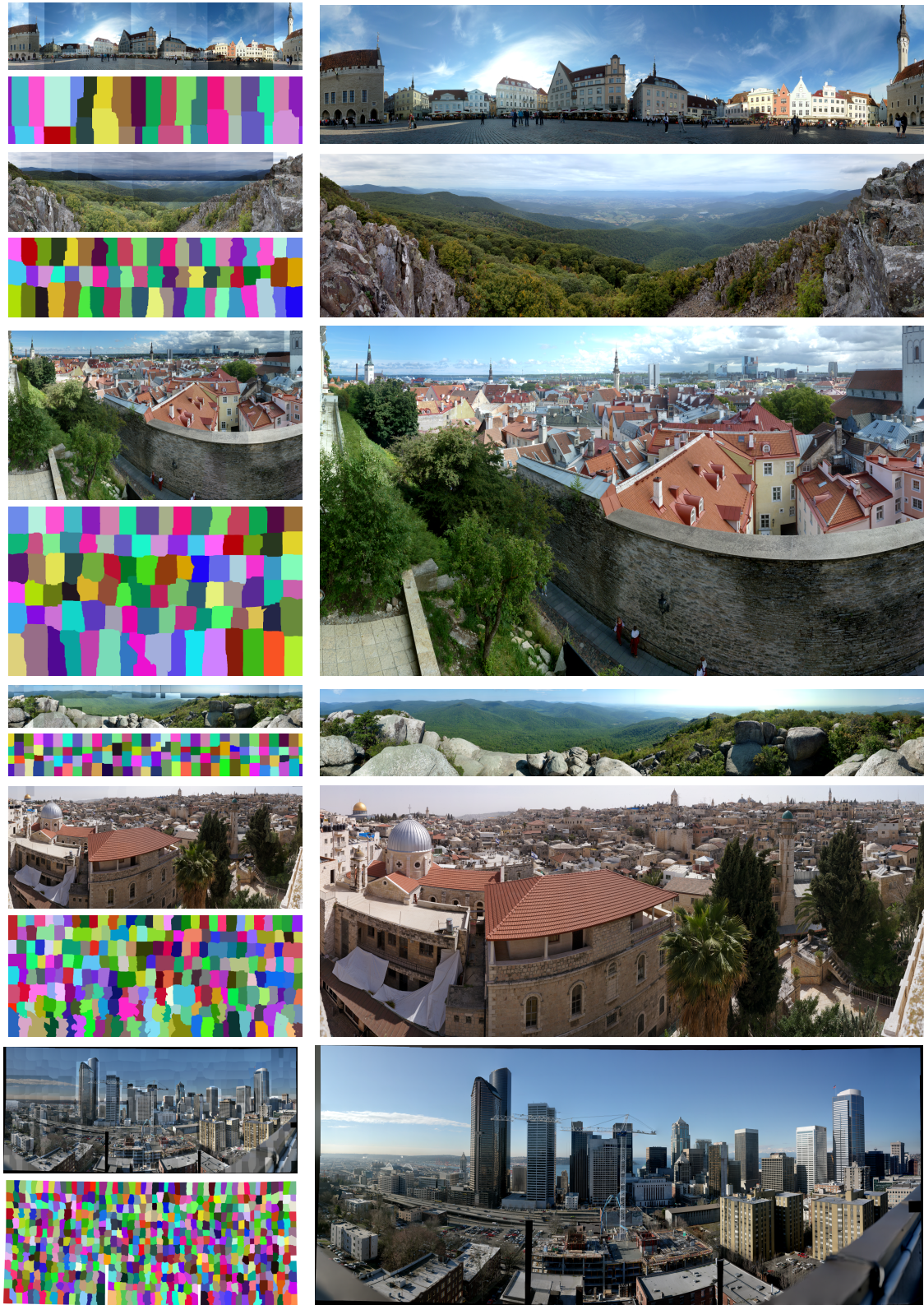


Figure 10: Image stitching results, showing the input composite and assignment mask making up the panorama (left), and the output (right).

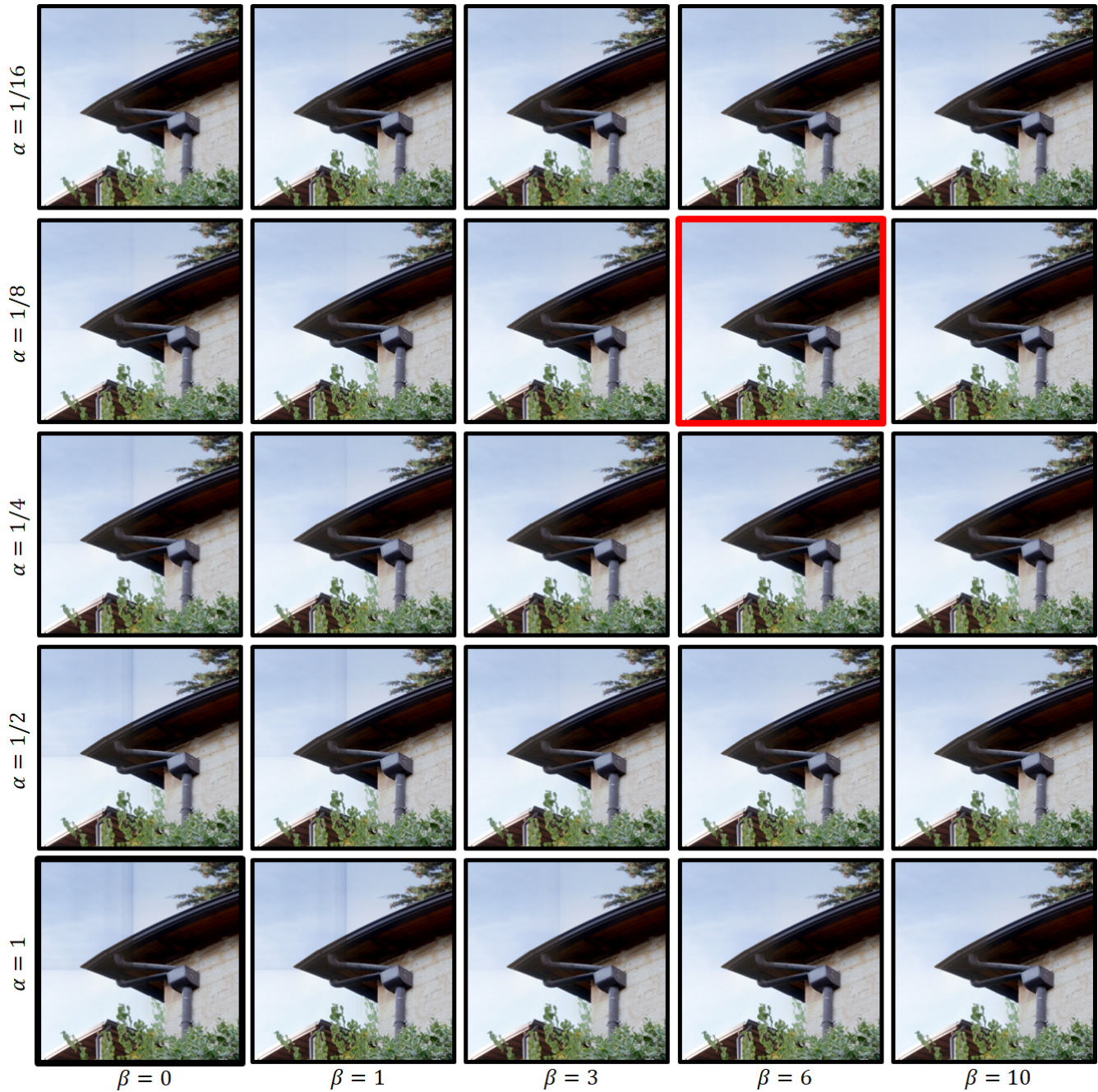


Figure 11: Close-ups from the Jerusalem panorama stitching results for different under-relaxation parameters α and β . (See Figure 7 in the main text for the full panorama.) Note that the bottom-left close-up corresponds to the result without under-relaxation and the close-up highlighted in red corresponds to the result with our default parameters.

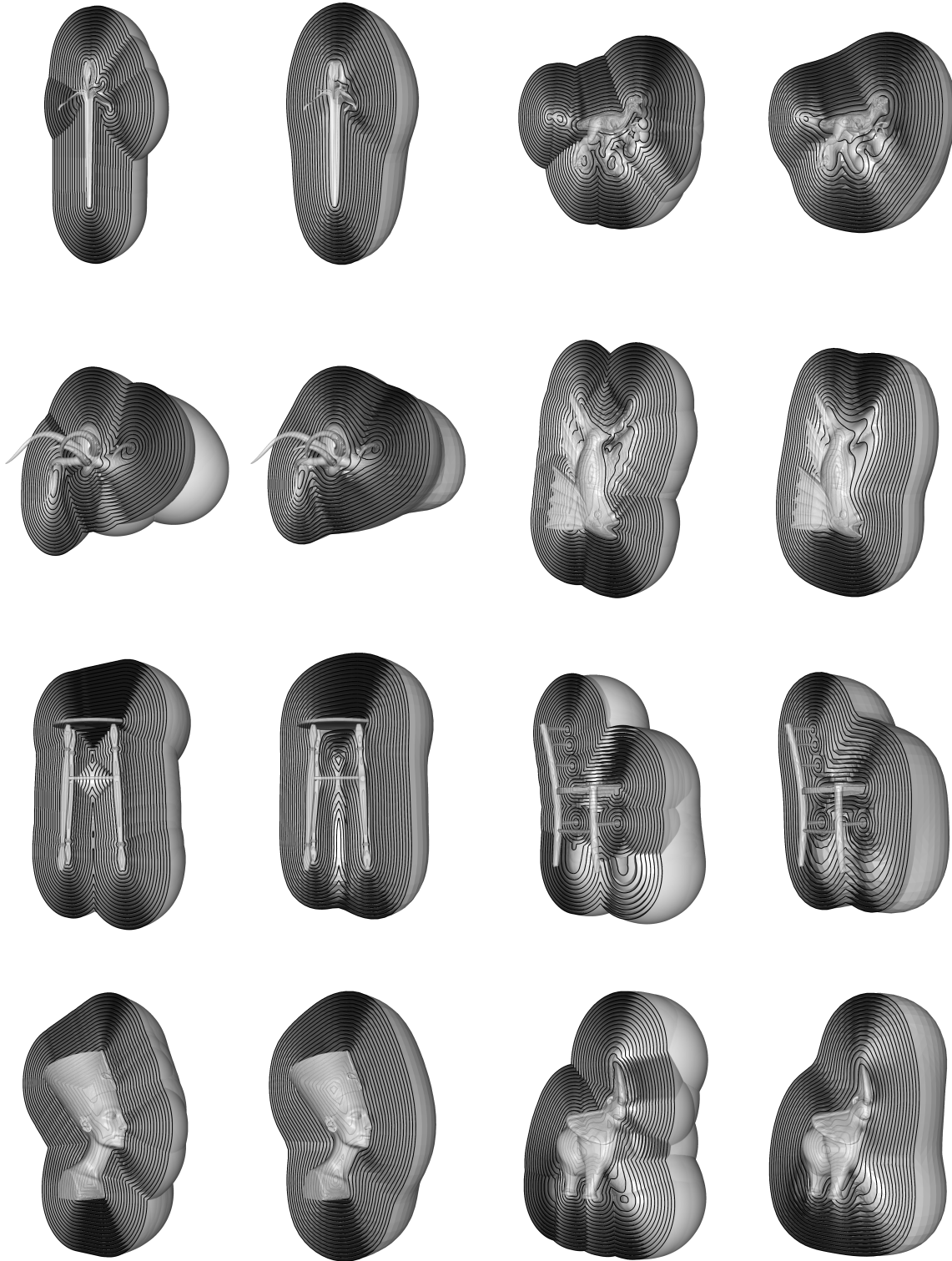


Figure 12: Isocontours of the Euclidean distance transform estimated using the method of Saito and Toriwaki (left) compared to the isosurfaces obtained by solving the Geodesics-In-Heat problem over an adaptive octree (right).

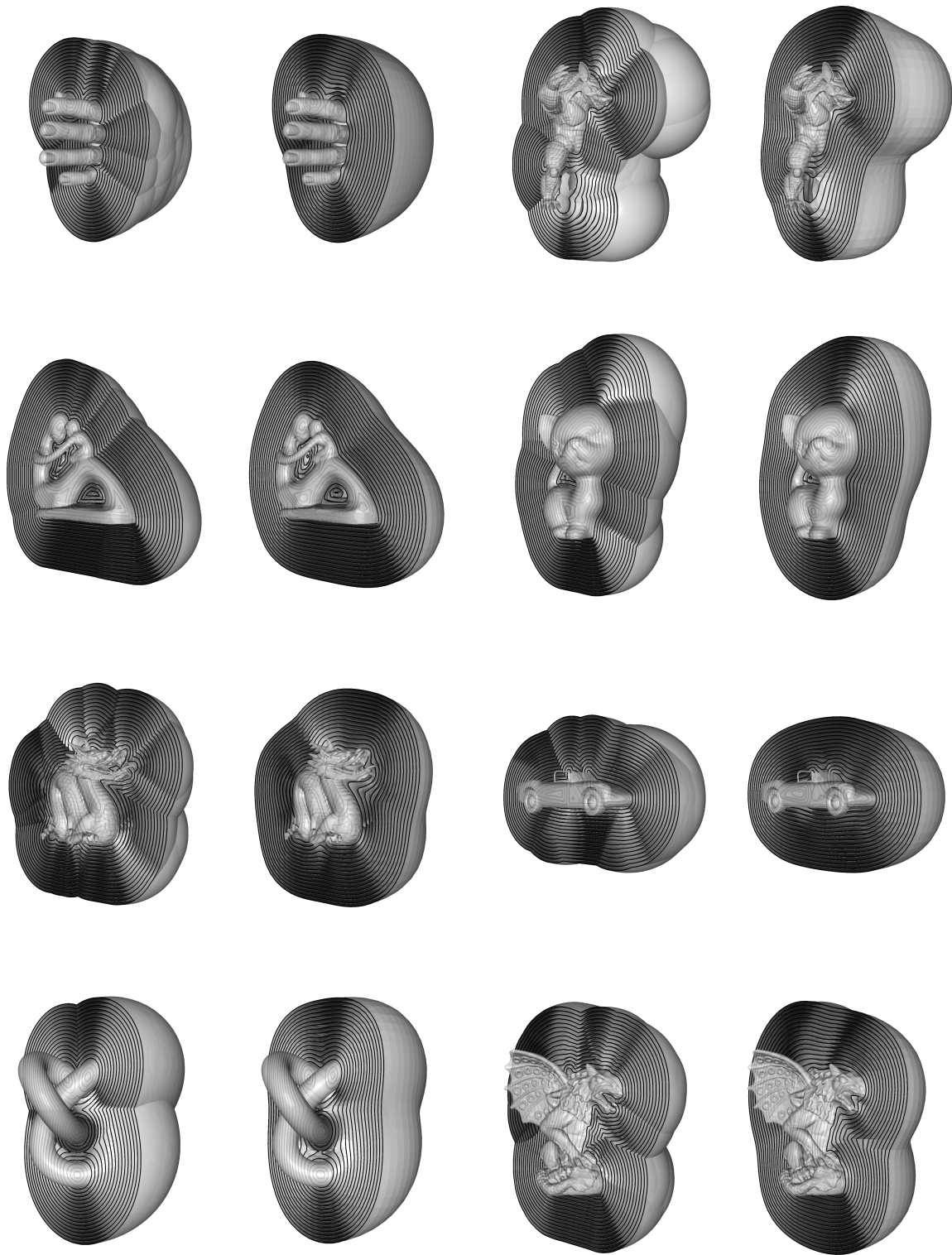


Figure 12: Isocontours of the Euclidean distance transform estimated using the method of Saito and Toriwaki (left) compared to the isosurfaces obtained by solving the Geodesics-In-Heat problem over an adaptive octree (right).

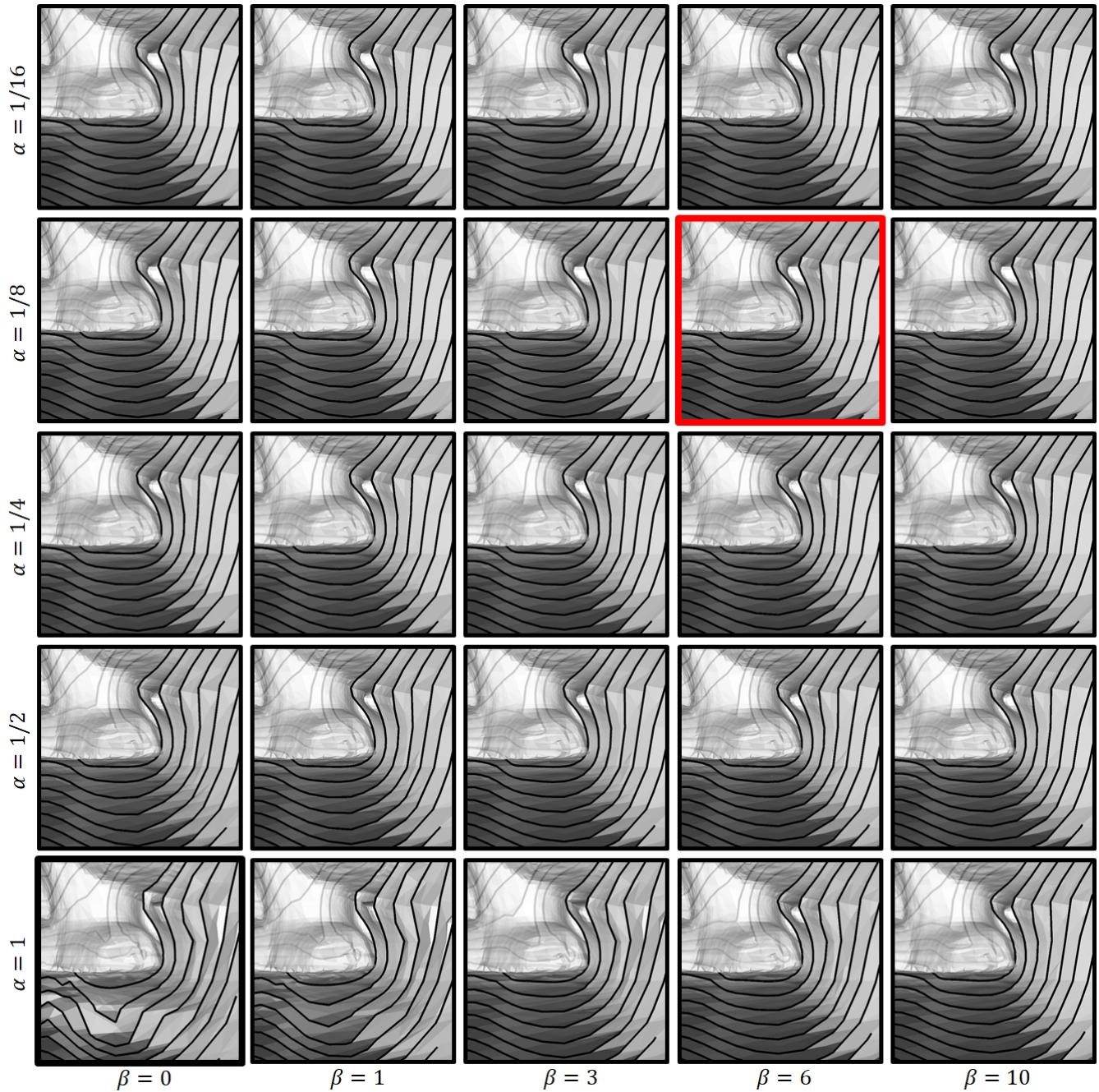


Figure 13: Close-ups from the isocontours of the Euclidean distance transform obtained from the bunny model for different under-relaxation parameters α and β . (See Figure 8 in the main text for the full panorama.) Note that the bottom-left close-up corresponds to the result without under-relaxation and the close-up highlighted in red corresponds to the result with our default parameters.